

Learned Image Compression with Discretized Gaussian-Laplacian-Logistic Mixture Model and Concatenated Residual Modules

Haisheng Fu, Feng Liang, Jianping Lin, Bing Li, Mohammad Akbari, Jie Liang, Guohe Zhang, Dong Liu, Chengjie Tu, Jingning Han

Abstract—Recently deep learning-based image compression methods have achieved significant achievements and gradually outperformed traditional approaches including the latest standard Versatile Video Coding (VVC) in both PSNR and MS-SSIM metrics. Two key components of learned image compression frameworks are the entropy model of the latent representations and the encoding/decoding network architectures. Various models have been proposed, such as autoregressive, softmax, logistic mixture, Gaussian mixture, and Laplacian. Existing schemes only use one of these models. However, due to the vast diversity of images, it is not optimal to use one model for all images, even different regions of one image. In this paper, we propose a more flexible discretized Gaussian-Laplacian-Logistic mixture model (GLMM) for the latent representations, which can adapt to different contents in different images and different regions of one image more accurately. Besides, in the encoding/decoding network design part, we propose a concatenated residual blocks (CRB), where multiple residual blocks are serially connected with additional shortcut connections. The CRB can improve the learning ability of the network, which can further improve the compression performance. Experimental results using the Kodak and Tecnick datasets show that the proposed scheme outperforms all the state-of-the-art learning-based methods and existing compression standards including VVC intra coding (4:4:4 and 4:2:0) in terms of the PSNR and MS-SSIM. The project page is at <https://github.com/fengyurenpingsheng/Learned-image-compression-with-GLMM>.

Index Terms—Deep learning-based image compression, Entropy coding, Gaussian Mixture Model, Residual Network.

I. INTRODUCTION

IMAGE compression is an important step in many applications. The classic compression standards, e.g., JPEG [1], JPEG 2000 [2], BPG (intra-frame encoding of HEVC)

Haisheng Fu, Feng Liang, Bing Li and Guohe Zhang are with the School of Microelectronics, Xi'an Jiaotong University, Xi'an, China (e-mail: fhs4118005070@stu.xjtu.edu.cn; fengliang@xjtu.edu.cn; libing888@stu.xjtu.edu.cn; zhangguohe@xjtu.edu.cn) (Corresponding author: Feng Liang)

Jianping Lin and Dong Liu are with the CAS Key Laboratory of Technology in Geo-Spatial Information Processing and Application System, University of Science and Technology of China, Hefei 230027, China (e-mail: ljp105@mail.ustc.edu.cn; dongeliu@ustc.edu.cn)

Mohammad Akbari and Jie Liang are with the School of Engineering Science, Simon Fraser University, Canada (akbari@sfu.ca; jiel@sfu.ca)

Chengjie Tu is with the Tencent Technologies (e-mail: chengjietu@tencent.com)

Jingning Han is with the Google Inc. (e-mail: jingning@google.com)

This work was supported in part by the National Natural Science Foundation of China (No. 61474093), in part by the Natural Science Foundation of Shaanxi Province, China (No. 2020JM-006), and in part by Tencent and Google.

[3], are mainly comprised of linear transform, quantization, and entropy coding. Recently, deep learning-based methods have been investigated, where the three main components are re-designed based on the properties of neural networks. This approach has gradually outperformed traditional methods in both PSNR and MS-SSIM metrics [4], and shows great potential.

The most important difference of learning-based schemes is that the classic linear transform is replaced by a non-linear neural network, which is learned from training data. Therefore, how to design the network architecture to reduce the correlation of the latent representations, which are the output of the encoding network (also known as the feature maps), is critical to the performance of learned image compression schemes. Another important task is to design a good entropy model to capture the remaining correlation of the latent representations, so that they can be encoded efficiently. In addition, how to design the quantization also affects the rate-distortion performance of the scheme greatly.

In the network design part, most schemes are based on the autoencoder framework, whose latent representations have much lower dimension than the input, and is very suitable for data compression. A powerful building block of many cutting-edge neural networks is the residual block first proposed in the ResNet [5], which uses shortcut connections to facilitate the design and training of deep networks, and can effectively improve the performances of many computer vision tasks. As a result, the residual block has also been used in many learning-based image compression schemes.

One of the first learned image compression schemes was proposed in [6], which was based on the recurrent neural network (RNN) and was used to compress thumbnail images.

In [7], [8] an encoder network that includes convolution, downsampling, and the generalized divisive normalization (GDN) is proposed. It was the first learned image compression scheme that achieved better performance than JPEG2000 in terms of both PSNR and MS-SSIM.

In [9], the residual block concept in [5] was used in the autoencoder architecture, which also achieved comparable performance to JPEG2000.

Generative adversarial network (GAN) is another powerful framework for many computer vision applications, and has also been used in several learned image coding schemes [10]–[12].

In [13], [14] a multi-resolution network architecture based

on the octave convolution in [15] is developed, which factorizes a feature map into a high-resolution and a low-resolution components, similar to the wavelet transform, which leads to improved rate-distortion performance.

In the entropy coding part, different entropy models have been proposed for the latent representations. In earlier schemes [8], [9], [16], [17], the quantized symbols are assumed to be independent and identically distributed (i.i.d.) and followed a simple marginal distribution, such as Gaussian scale mixture (GSM) (zero-mean Gaussian with different scales). Once these distribution parameters are fully trained, the probability table of the latent representations is fixed in encoding and decoding, which are used by the entropy coding to losslessly compress the quantized latents. Since the entropy model is overly simplified, the performances of these methods are compromised.

To improve the entropy model, the hyperprior approach is developed. In [18], the authors proposed to estimate the probability distribution of the latent representations with a GSM model, where the scale parameter is estimated by a hyperprior module, which is coded and sent to the decoder. This achieves adaptive entropy coding for different images, which allows it to get better performance than BPG (4:4:4).

In [19], the Gaussian mixture model (GMM) is proposed for the hyperprior. In addition, an autoregressive context model is introduced to predict each latent representation from its causal context.

In [20], to minimize serial processing, the latent representations are split into two slices. The first slice is coded using a Gaussian entropy model and a hyperprior. The second slice is coded using both the hyperprior and the decoded symbols in the first slice.

Other models have been used for latent representations. For example, PixelCNN [21] employs 256-way softmax distribution to predict each pixel, but its complexity is very high. In [22], the PixelCNN++ is proposed, which uses the discretized logistic mixture distribution to simplify the complexity of [21]. In [23], PixelCNN++ is applied to lossless image compression. In [24], the Laplacian distribution was used for lossy compression, which achieved the highest PSNR and MS-SSIM performance for low bit-rate in 2019 CVPR Workshop and Challenge on Learned Image Compression (CLIC) [25].

In [26], the GMM model is also adopted in the hyperprior coding. It also uses a quality enhancement subnetwork to improve the performance. It is the first learned image compression approach that achieves better performance than VVC (4:4:4) in both PSNR and MS-SSIM. As far as we know, the results in [26] are currently the best in the literature.

In the quantization part, the attention mask is used in [27] to adjust bit allocation in different regions based on the image content, but the mask also needs to be sent to the decoder. In [28], non-local attention module is used to generate attention mask without sending side information, and it is used in both image coding and hyperprior coding. In [29], the attention module in [28] is simplified. The GMM model is also used in [29] in the hyperprior coding. Comparable performance to VVC (4:4:4) in PSNR is achieved in [29].

Although the learned methods have made significant progresses, the compression performance can be further improved.

First, the previous entropy model methods only use a single distribution, which is not optimal for every image. Second, the latent representations still exist some spatial redundancy. In order to address these issues, we make the following contributions in this paper:

- Instead of using a single probability distribution model, we propose a discretized Gaussian-Laplacian-Logistic mixture model, which is much more flexible and accurate in estimating the probability distributions of the latent representations. Ablation studies demonstrate that the proposed joint model outperforms all previously proposed single models. For example, it achieves 0.1-0.15 dB gain in PSNR compared to the GMM model for the Kodak dataset.

- We improve the basic building block of the encoder network by developing a concatenated residual module (CRM), with additional shortcut connections. The CRM improves the information flow, reduces the correlation of the output, and improves the training of the network. Ablation studies using the Kodak dataset show that the proposed CRM can achieve 0.2-0.3 dB gain in terms of PSNR compared to the original residual blocks. We also conduct ablation studies to compare the performances of CRMs with two and three stages of residual blocks.

- One of the key contributions of [26] is the post-processing component, which achieves 0.5 dB gain in [26] compared to its baseline. We also investigate the performance of this component in our scheme. However, our experiments show that there is no need to apply the post-processing in our method, because the proposed CRM and entropy model have done a good job. This also reduces the complexity of the scheme.

- Experimental results using the Kodak [30], Tecnick [31] datasets show that the proposed scheme outperforms all the previous learning-based methods including [26] and traditional codecs including VVC in terms of the PSNR and MS-SSIM. For example, for the Kodak dataset in terms of PSNR, when the bit rate is higher than 0.4 bpp, our method is 0.2-0.3 dB higher than [26], [29], and 0.3-0.4 dB higher than VVC(4:4:4). For the Tecnick dataset, in terms of PSNR, when the bit rate is higher than 0.2 bpp, our method is 0.3-0.4 dB higher than VVC(4:4:4). This represents the new state of the art in learned image compression.

The remainder of the paper is organized as follows. In Section II, we propose our image compression framework with discretized Gaussian-Laplacian-Logistic mixture model and the concatenated residual modules (CRM). In Sec. III, we compare our methods with some traditional state-of-the-art learning-based methods and classical image compression methods. Ablation experiments are carried out to investigate the performance gain of the proposed scheme. The conclusions are reported in Sec. IV.

II. THE PROPOSED IMAGE COMPRESSION FRAMEWORK

In this section, we first describe the overall structure of the proposed framework, and then explain the details of important components, including the encoder/decoder networks, the concatenated residual module (CRM), the discretized Gaussian-

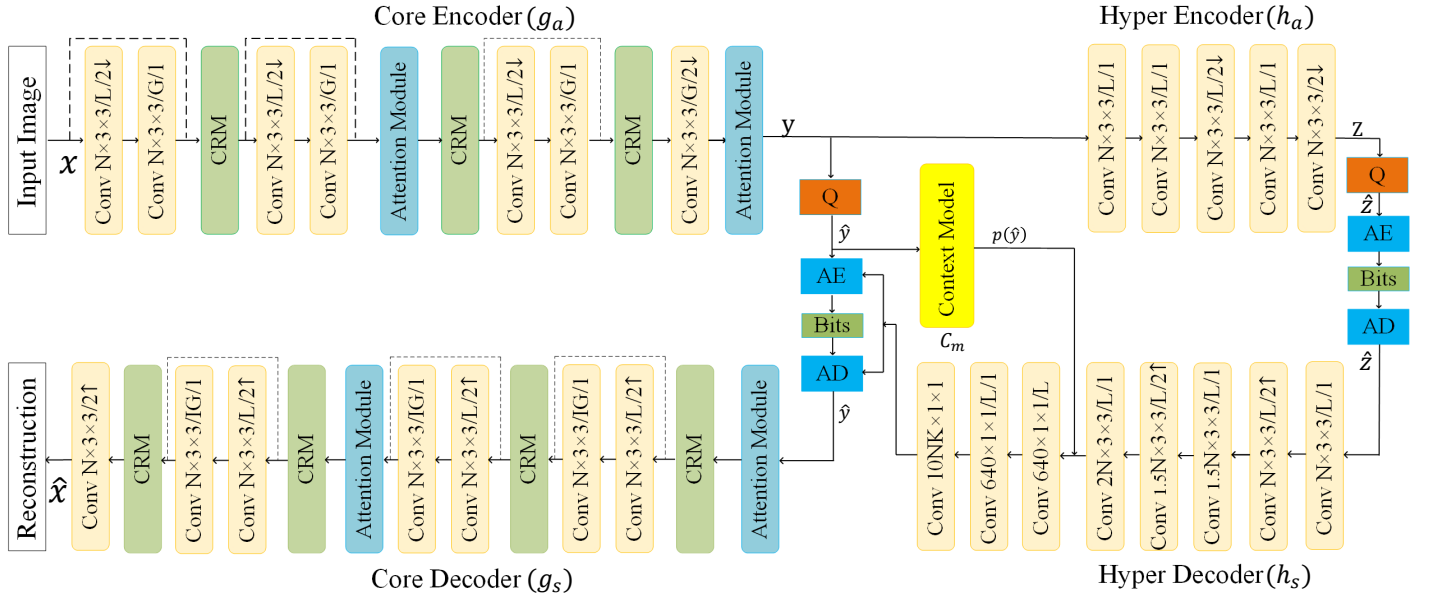


Fig. 1. The Framework of the proposed image compression scheme. G and IG represent the GDN module and inverse GDN module, respectively. \uparrow and \downarrow denote the up- or down- sampling. 3×3 is the size of convolution kernel. AE and AD represent the arithmetic encoder and arithmetic decoder, respectively. The L represents leaky ReLU. The dotted lines denote the shortcut connection with size change, as in [5], [29].

Laplacian-Logistic mixture model (GLLMM), and the objective function.

A. Overview of the Framework

The block diagram of the proposed scheme is illustrated in Fig. 1, which is mainly based on [29]. It is comprised of the core autoencoder part, the hyperprior coding part, and the autoregressive context model. The core autoencoder part includes an encoder (g_a) and a decoder (g_s). The hyperprior coding part consists of a hyper encoder (h_a) and a hyper decoder (h_s). There are two modifications from [29]. First, we propose a concatenated residual module (CRM) to replace some residual blocks in the core encoder/decoder. Second, we propose a new Gaussian-Laplacian-Logistic mixture model to replace the Gaussian mixture model in the hyperprior coding.

The input image x is first sent to the encoder network (g_a), which aims to reduce the pixel-wise redundancy of the input image, and learn a latent representation (y) of the input image. The latent representation is then quantized and entropy coded. The quantized latent representation is denoted by \hat{y} , which is coded by context-adaptive entropy coding. To do this, y is first sent to the hyper encoder h_a to estimate its distribution. The output z of the hyper encoder h_a is encoded as a side information to the decoder without building a prior probability model.

To further improve the entropy coding efficiency, two other techniques are adopted. First, the autoregressive context model c_m is used to predict each latent representation from its causal context [19]. The probability distribution of \hat{y} is estimated by combing the autoregressive context model and the output of the hyper decoder, which is then used to encode \hat{y} . Second, the attention module is used in the core autoencoder to adjust bit allocation in different regions [29].

Since autoregressive context model is used, the symbols have to be decoded in serial manner. After all the symbols of \hat{y} are decoded, they are sent to the core decoder (g_s) to generate the reconstructed image.

B. Network Architecture

In Fig. 1, the size of the input image X is $W \times H \times 3$, where W and H represents the width and height of the source image, respectively. In the training of the network, the data of the source image are normalized to $[-1, 1]$ by $(\frac{X}{127.5} - 1.0)$. The analysis transforms and synthesis transforms in the core and hyper networks are symmetric, except that they use convolution and deconvolution operators, respectively.

As in [29], the core encoder network includes various convolution layers and four stages of pooling operators to get the low-dimensional latent representations. The residual blocks with shortcut connections are used extensively, as in ResNet [5]. The GDN operator is used when the size is changed, as in [29].

The simplified attention module in [29] is applied at two resolutions to strengthen more important areas, so that they will get more bit allocation. The structure of the attention module is shown in Fig. 2.

When the size does not change, to further remove the spatial correlation in the latent representation, we develop two deeper residual blocks in this paper, which is illustrated in Fig. 3. The basic building block is the standard residual block developed in the ResNet [5], as described in Fig. 3(a). As in [29], we first employ the leaky ReLU activation function to replace the ReLU function and remove the batch normalization layer from the residual block. The leaky ReLU activation function can speed up the convergence of the network. The detailed structure is shown in Fig. 3(b), which is used in [29]. Based

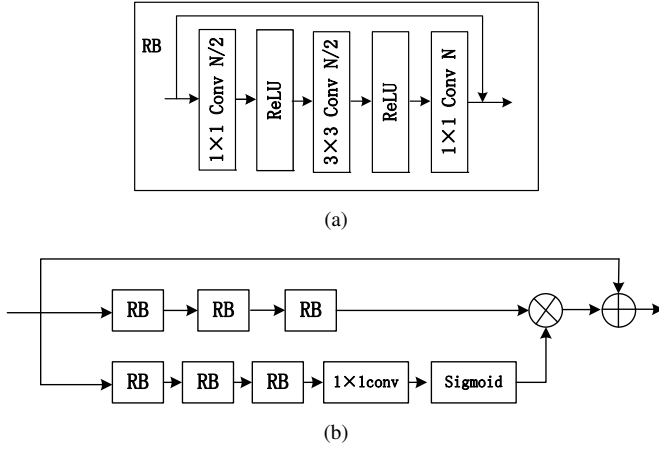


Fig. 2. (a) Residual block [5]; (b) The attention module in [29].

on this, we develop two concatenated residual modules, as shown in Fig. 3(c) and Fig. 3(d).

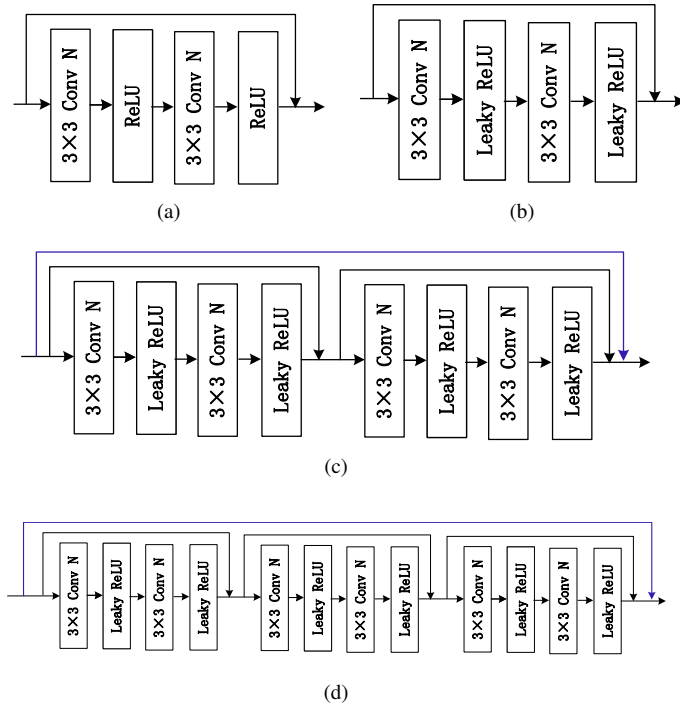


Fig. 3. (a) The standard residual block; (b) the residual block with Leaky ReLU; (c) the proposed two-stage concatenated residual module; (d) the proposed three-stage concatenated residual module.

In Fig. 3(c), two residual blocks in Fig. 3(b) are concatenated, and another short connection is added between the input and the output. In Fig. 3(d), three residual blocks are concatenated, with an additional shortcut connection as well.

Compared to the standard residual block in Fig. 3(b), the concatenated modules have larger receptive fields. They can remove more spatial correlation, which can also help the attention module in the network. In Sec. III, we will compare the performances of the two types of concatenated modules.

The network in the hyperprior coding part is similar to that in [19], [29]. Since the input dimension is much lower than the

original image, the network is much simpler than that in the core coding part. Leaky ReLU is utilized in most convolution layers, except for the last layer in hyperprior encoder and decoder, which do not have any activation function.

C. Proposed Gaussian-Laplacian-Logistic Mixture Model (GLLMM)

In an end-to-end learning-based image compression framework, the processing of the image compression in Fig. 1 can be represented by Eq. (1).

$$\begin{aligned} y &= g_a(x; \phi) \\ \hat{y} &= Q(y) \\ \hat{x} &= g_s(\hat{y}; \theta) \end{aligned} \quad (1)$$

where x , \hat{x} , y , \hat{y} represent the origin image, decompressed image, the latent representation before quantification and the latent representation after quantification, respectively. ϕ and θ are parameters that need to be optimized in the encoder network and decoder network, respectively. Fig. 1 can be simplified into the block diagram in Fig. 4(a), where in the training procedure, $U \mid Q$ denotes the uniform quantization procedure and entropy coding. As in [18], a uniform noise $U(-\frac{1}{2}, \frac{1}{2})$ is added to y to obtain noisy codes \tilde{y} for better training. In the inference procedure, y is quantized to \hat{y} . The \hat{y} is encoded into the bitstream via entropy coding.

As discussed before, once the training of the coding frameworks is complete, the parameters of the networks are fixed. During encoding and decoding procedure, a fixed probability distribution is used to code \hat{y} for all test images. This is clearly not optimal. Therefore it is necessary to introduce adaptive entropy model to improve the performance.

In [18], the hyperprior method is introduced, as shown in Fig. 4(b), where h_a and h_s represent the hyper encoder and hyper decoder in the hyper autoencoder. The ϕ_h and θ_h are needed optimized network parameters. \hat{z} is transmitted as side information, which should be quantized and compressed. $P_{\hat{y}|\hat{x}}(\hat{y}|\hat{x})$ represents different distributions conditioned on \hat{z} . The decoder first recovers \hat{z} from compressed signal and uses h_s to obtain the probability distribution parameter of the latent representation \hat{y} . The \hat{y} is recovered according to the known probability distribution parameters. It then feeds \hat{y} into g_s to generate the the reconstructed image.

Unlike the frameworks in Fig. 4(a), the probability distributions of the latent representation y in Fig. 4(b) to Fig. 4(d) are conditioned on \hat{z} . That is, the probability distribution parameters of y are adaptive, and the value of the probability distribution parameters $P_{\hat{y}|\hat{x}}(\hat{y}|\hat{x})$ can be adaptively changed according to the different test images, which can better capture spatial redundancy of y .

In [18], $P_{\hat{y}|\hat{x}}(\hat{y}|\hat{x})$ is assumed to follow the zero-mean Gaussian distribution with scale parameters $\sigma^2 = h_s(\hat{z}; \theta_h)$. The relationships in Fig. 4(b) can be written as:

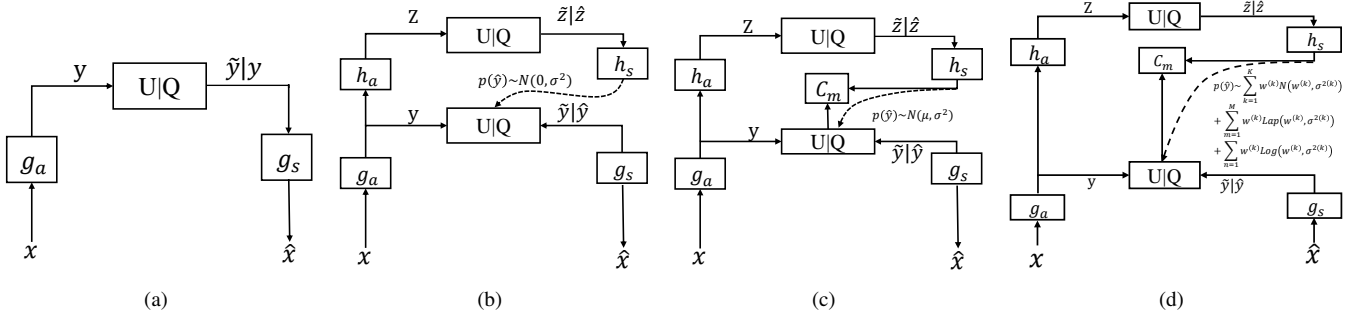


Fig. 4. Different learning-based image coding frameworks. (a) Framework with fixed entropy model [8]; (b) Framework in [18] with Hyperprior; (c) Framework in [19] with Gaussian model; (d) Proposed Framework.

$$\begin{aligned}
 z &= h_a(y; \phi_h) \\
 \hat{z} &= Q(z) \\
 P_{\hat{y}|\hat{x}}(\hat{y}|\hat{x}) &\leftarrow h_s(\hat{z}; \theta_h) \\
 P_{\hat{y}|\hat{x}}(\hat{y}|\hat{x}) &\sim N(0, \sigma^2)
 \end{aligned} \tag{2}$$

$P_{\hat{y}|\hat{z}}(\hat{y}|\hat{z})$ in Eq. (2) are for continuous values, but \hat{z} is discrete-valued after quantization. The authors in [18] utilize the discretized zero-mean Gaussian distribution. The entropy model is thus formulated as

$$\begin{aligned}
 P_{\hat{y}|\hat{z}}(\hat{y}|\hat{z}) &= \prod_i (P_{\hat{y}_i|\hat{x}_i}(\hat{y}_i|\hat{x}_i)) \\
 &= N(0, \sigma_i^2)
 \end{aligned} \tag{3}$$

where i represents the location index in feature tensor. For example, \hat{y}_i is the i -th symbol of the latent representation \hat{y} and σ_i represents the i -th element of σ .

As in [18], the \hat{z} has no prior information, the factorized density model ϕ is employed to encode \hat{z} as

$$p_{\hat{z}|\psi}(\hat{z}|\psi) = \prod_i (p_{z_i|\psi}(\psi) * U(-\frac{1}{2}, \frac{1}{2})(\hat{z}_i)) \tag{4}$$

To make the quantization step differentiable in the training, uniform noises $U(-\frac{1}{2}, \frac{1}{2})$ are added to the latent representation y and z , as in [18]. The uniform quantization is employed to the latent representations during inference.

In [19], a more accurate entropy model is proposed, which jointly utilizes an autoregressive context model and a mean and scale hyperprior. The scheme can be represented by Fig. 4(c), where C_m is the context model. The context model can exploit the masked convolution to reduce the redundancy of the latent representation and improves the compression performances. $P_{\hat{y}|\hat{x}}(\hat{y}|\hat{x})$ is assumed to follow a non-zero mean Gaussian distribution with scale parameters $\sigma^2 = h_s(\hat{z}; \theta_h)$, as shown in Eq 5:

$$P_{\hat{y}|\hat{x}}(\hat{y}|\hat{x}) \sim N(\mu, \sigma^2) \tag{5}$$

Based on [19], in [29], a more accurate entropy model, based on the autoregressive context model and discretized Gaussian mixture distribution is proposed, as shown in Eq.

6, the weighted average of multiple Gaussian models with different means and variances is used to estimate $P_{\hat{y}|\hat{x}}(\hat{y}|\hat{x})$, which can represent the actual distributions more accurately than a single model.

$$P_{\hat{y}|\hat{x}}(\hat{y}|\hat{x}) \sim \sum_{k=1}^K w^k N(\mu^{(k)}, \sigma^{2(k)}) \tag{6}$$

Models with other distributions have also been investigated, such as the softmax distribution in [21], logistic mixture model in [22], [23], and Laplacian distribution in [24].

However, the aforementioned methods only use one type of probability model to learn the probability distribution of the latent representation. It is difficult for one probability model to learn the distributions of all images. Therefore, it is necessary to combine different types of distributions in the modeling.

In this paper, we propose a powerful discretized Gaussian-Laplacian-Logistic model (GLLMM) distribution with different means and scales, as shown in Fig. 4(d) and Eq. 7.

$$\begin{aligned}
 P_{\hat{y}|\hat{x}}(\hat{y}|\hat{x}) &\sim p_0 \sum_{k=1}^K w^k N(\mu^{(k)}, \sigma^{2(k)}) \\
 &+ p_1 \sum_{m=1}^M w^m Lap(\mu^{(m)}, \sigma^{2(m)}) \\
 &+ p_2 \sum_{n=1}^N w^n Logi(\mu^{(n)}, \sigma^{2(n)})
 \end{aligned} \tag{7}$$

where p_i represents the probability occupied by each distribution, $Lap()$ represents the Laplacian distribution, $Logi()$ represents the logistic distribution, and the values of K , M , and N are set to 3.

Compared to the previous models with a single type of distribution, the proposed joint model includes three types of distributions, and can capture the distribution of the latent representations more accurately, thereby improving the performance.

Eq. (7) is also for continuous values, but \hat{y} is discrete-valued after quantization. To make it more accurate, we use the discretized Gaussian-Laplacian-Logistic mixture distribution. The entropy model is thus formulated as

$$\begin{aligned}
P_{\hat{y}|\hat{z}}(\hat{y}|\hat{z}) &= \left(\prod_i (P_{\hat{y}_i|\hat{x}}(\hat{y}_i|\hat{x})) \right) \\
P_{\hat{y}_i|\hat{z}}(\hat{y}_i|\hat{z}) &= p_0 \left(\sum_{k=1}^K w_i^k N(\mu_i^{(k)}, \sigma_i^{2(k)}) \right) \\
&\quad + p_1 \sum_{m=1}^M w_i^m \text{Lap}(\mu_i^{(m)}, \sigma_i^{2(m)}) \\
&\quad + p_2 \sum_{n=1}^N w_i^n \text{Logi}(\mu_i^{(n)}, \sigma_i^{2(n)}) * U\left(-\frac{1}{2}, \frac{1}{2}\right) \\
&= c\left(\hat{y}_i + \frac{1}{2}\right) - c\left(\hat{y}_i - \frac{1}{2}\right)
\end{aligned} \tag{8}$$

As in [24], [29], the c represents the cumulative function.

D. Loss Function

The learning-based image compression needs to optimize the rate-distortion performance. Let R be the expected length of the bitstream, and D be the reconstruction error between the source image and reconstructed image. The tradeoff between the rate and distortion is adjusted by a Lagrange multiplier denoted by λ . The objective cost function is then defined as follows:

$$\begin{aligned}
L &= \lambda D(x, \hat{x}) + H(\hat{y}) + H(\hat{z}). \\
H(\hat{y}) &= E[-\log_2(P_{\hat{y}|\hat{z}}(\hat{y}|\hat{z}))] \\
H(\hat{z}) &= E[-\log_2(P_{\hat{z}}(\hat{z}))]
\end{aligned} \tag{9}$$

where $D(x, \hat{x})$ is the reconstruction error between origin image x and the decompressed image \hat{x} , such as mean square error (MSE) and MS-SSIM. $H(\hat{y})$, $H(\hat{z})$ are the entropies of the core latent representation and hyper representations.

III. EXPERIMENT

In this section, we compare our method with different learning-based methods and existing compression standards in terms of both PSNR and MS-SSIM metrics when measured on the Kodak PhotoCD dataset [30] and Tecnick dataset [31]. The Kodak dataset consists of 24 images with a resolution of 768×512 or 512×768 . The Tecnick dataset is comprised of 100 uncompressed images with a resolution of 1200×1200 . The learning-based methods are recent state-of-the-art methods, including Balle2017 [8], Li2018 [27], Lee2019 [32], Lee2020 [26], Li2020 [33], and Cheng2020 [34]. We also compare with traditional methods, including VVC-Intra (4:4:4) [35], VVC-Intra (4:2:0), BPG (4:4:4) [3], JPEG2000, WebP [36], and JPEG. Both PSNR and MS-SSIM metrics are used. The original MS-SSIM values are represented in dB scale by $-10 \log_{10}(1 - MS-SSIM)$.

A. Training Set

The CLIC dataset [37] and LIU4K dataset [38] are employed to train our models. The images of the training dataset are rescaled to a resolution of 2000×2000 , which is better for training. Data augmentation algorithms (i.e., rotation and scaling) are deployed to randomly cropped 81,650 patches with a resolution of 384×384 . The patches are stored as lossless PNG images for better training.

B. Parameter Settings

We optimize the proposed models using mean square error (MSE) and MS-SSIM respectively. When optimized for MSE metric, the parameter λ is selected from the set $\{0.0016, 0.0032, 0.0075, 0.015, 0.023, 0.03, 0.045\}$. Each value trains a network for a particular bit rate. The number of filters N is set to 128 for the three lower bit rates, and is set to 256 for the four higher bit rates. When the MS-SSIM metric is targeted, the parameter λ is in the set $\{12, 40, 80, 120\}$. The number of filters N is set to 128 for the two lower bit rate, and is set to 256 for the two higher bit rates. Each model was trained up to 1.5×10^6 iterations to obtain stable performance. The Adam solver with a batch size of 8 is adopted. The learning rate is set to 1×10^{-4} in the first 750,000 iterations, and we gradually reduce the learning rate by 0.5 after every 100,000 iterations in the last 750,000 iterations.

C. Performance Comparisons

The average MS-SSIM and PSNR performances over the 24 Kodak images are illustrated in Fig. 5. When optimized for PSNR, Lee2020 (PSNR) [26] is the best among previous methods, which obtains even better performance than VVC (4:4:4) at high rates. The next closest method to VVC4:4:4 is Cheng2020 [29]. When the bit rate is less than 0.3 bpp, our method has similar performance to [26] and VVC4:4:4. When the bit rate is higher than 0.4 bpp, our method achieves the best performance, which is 0.2-0.3 dB over [26] and 0.3-0.4 dB over VVC4:4:4.

In the MS-SSIM results in Fig. 5(b), Lee2020 (MS-SSIM) [26] also achieves better performance than previous learning-based methods and all the traditional image codecs including VVC (4:4:4). Our proposed method optimized for MS-SSIM achieves slightly better results than Lee 2020 (MS-SSIM).

We also evaluate the performance of the proposed method on the Tecnick dataset and compare to other methods. The results are shown in Fig. 6. The results of some methods are not available for the Tecnick dataset. It can be seen that our scheme also outperforms all the learning-based methods including Lee2019 [32] and all the traditional image codecs including VVC (4:4:4) in term of both PSNR and MS-SSIM. When the bit rate is above 0.2bpp, our method is about 0.2-0.3 dB higher than VVC4:4:4.

Three examples are shown in Fig. 8 to Fig. 9 to compare the visual quality of different methods. Our method produces the most visually pleasing results.

D. Ablation Studies of Different Modules

We carry out the first ablation study to examine the performance gain of different modules, including concatenated residual module (CRM), and the discretized Gaussian-laplace-Mixture model. As a baseline, we replace the CRM with the standard residual block (as shown in Fig. 3(a)), and the discretized Gaussian-Laplacian-Logistic mixture model is replaced with discretized Gaussian Mixture model. Based on the baseline, we add different modules in turn. In order to compare as fair as possible, the parameter λ is chosen in the set $\{0.0032, 0.0075, 0.015, 0.03, 0.045\}$. The number of filters

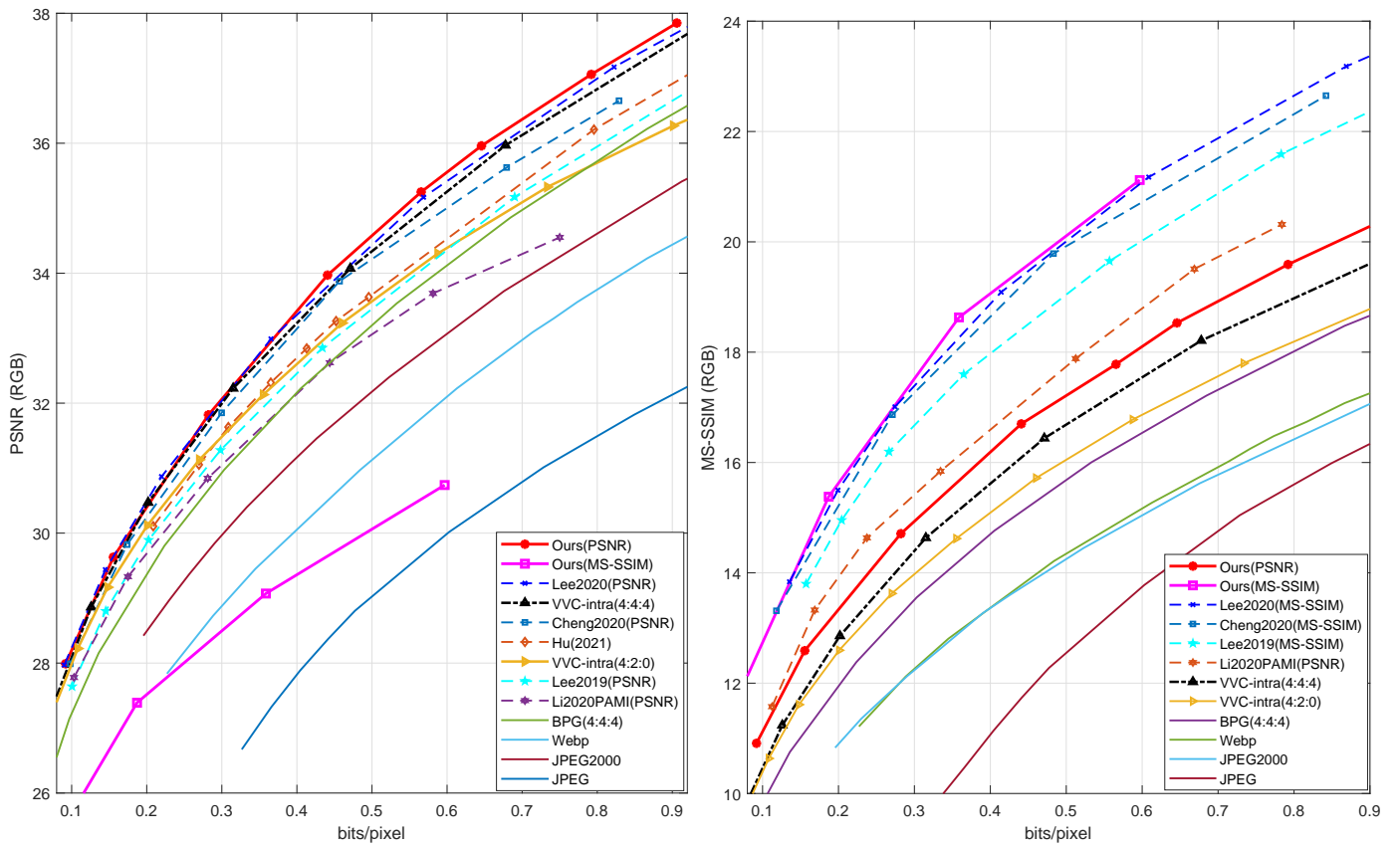


Fig. 5. Average PSNR and MS-SSIM comparison results on all 24 Kodak images.

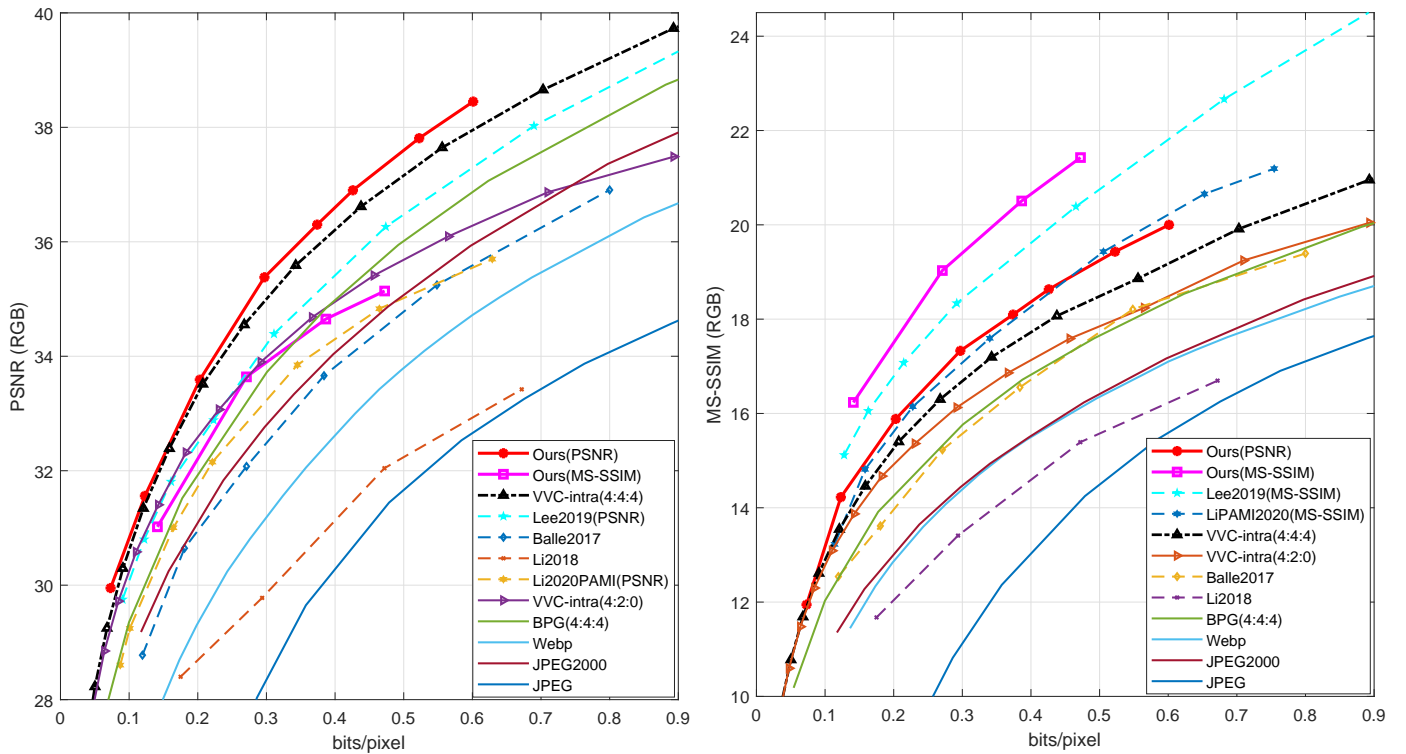


Fig. 6. Average PSNR and MS-SSIM evaluation results on all 100 uncompressed Tecnick images.

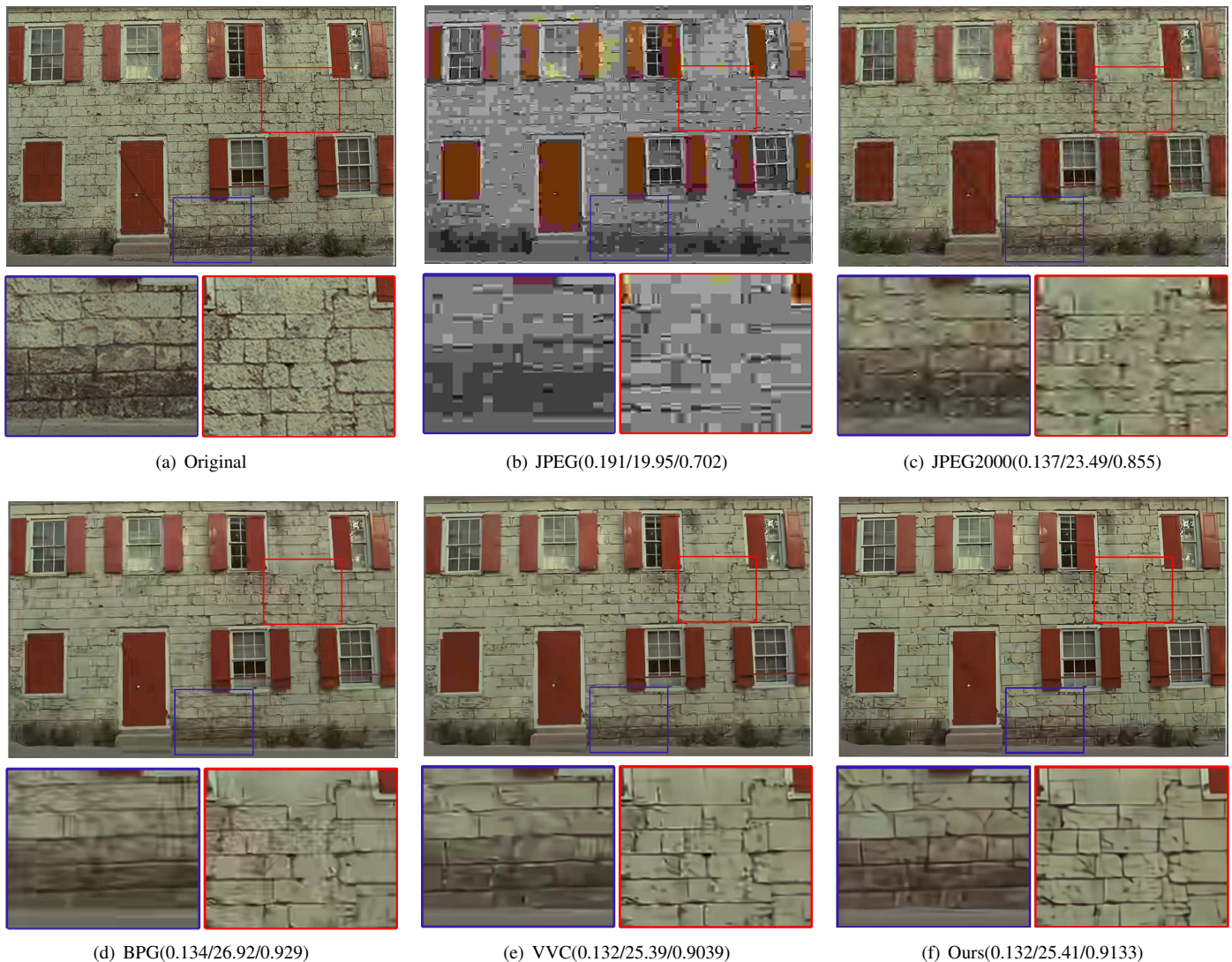


Fig. 7. Example 1 in the Kodak dataset (bpp, PSNR (dB), MS-SSIM).

N is set to 128 for the two lower bit rates, and is set to 256 for the three higher bit rates. Other training setups are the same. The MSE objective function is optimized in the ablation experiments.

The results are shown in Fig. 10. We first employ GLLMM to replace the GMM in the baseline, denoted as Baseline+GMM, which improves the R-D performance about 0.15 dB at the same bit rate. Compared to Baseline+GMM, the proposed full method in this paper has a further improvement of 0.3 dB, which is the contribution of the CRM over the original residual blocks.

We next investigate different combinations of probability distributions, including Gaussian mixture model (GMM), Gaussian + Logistic mixture model (GLoMM), Gaussian + Laplacian mixture model (GLaMM), and the proposed Gaussian + Logistic + Laplacian mixture model (GLLMM). If some distributions are not used, we set the corresponding M , N or K in Eq. (7) to 0. The results are illustrated in Fig. 11. The method with GMM achieves the worst performance. GLaMM is slightly better than GMM, and GLoMM is further better

than GLaMM, and is 0.05 dB higher than GMM. The full GLLMM is about 0.15 dB higher than GMM at all bit rates.

E. Performance Improvement of Different Concatenated Residual Modules

We investigate the performances of different concatenated residual modules on image compression scheme, including the standard residual block (RB), two-stage concatenated residual module (RB+two-stage) and three-stage concatenated residual module (RB+three-stage). The results are shown in Fig. 12.

The method with RB [5] achieves the worst performance. RB+two-stage method is 0.3 dB higher than RB. The RB+three-stage achieves the same performance with RB+two-stage at low bit rates and is slightly worse at high bit rates. Moreover, the model size will increase about 13 %. Therefore, we adopt the RB+two-stage method in our framework.

F. Effectiveness of post-processing module

We also study the effectiveness of the post-processing module on image compression performance in our method.



Fig. 8. Example 2 in the Kodak dataset (bpp, PSNR (dB), MS-SSIM).

In [26], the post-processing module is combined to the image compression framework, which achieves 0.5 dB gain compared to its baseline without the post-processing. The post processing can be applied to other learning-based schemes as well. To study its effectiveness in our scheme, we implement the same post-processing as in [26] into our method. The corresponding results are listed in Table I. We can observe that these two schemes have almost the same performances on Kodak dataset. The main reason is that we have much better residual modules and entropy model. Therefore there is no need to apply the post processing. This also reduces the complexity of the scheme.

IV. CONCLUSION

In this paper, we improve the state of the art of learning-based image compression by presenting a more flexible entropy model based on the discretized Gaussian-Laplacian-Logistic mixture distribution, which captures the spatial correlation more effectively in latent representations. We also develop an improved concatenated residual block module for the encoder network.

Experiments demonstrate that the proposed method outperforms VVC (4:4:4) in terms of both PSNR and MS-SSIM metric when measured on kodak and Tecnick dataset. Also, our scheme achieves better performance compared to all the previous state-of-the-art learning-based methods.

Our method still has some rooms to improve. Since the context model is employed in our framework, the symbols have to be decoded in a serial manner. Although it can effectively reduce the spatial correlation of the latent representation, it significantly increases the time complexity. How to reduce the complexity of the context model without too much degradation of the performance is a future research topic. Also, the complexity of our method can be further optimized by different approaches such as model compression and optimization.

REFERENCES

- [1] G. K. Wallace, "The jpeg still picture compression standard," *IEEE Transactions on Consumer Electronics*, vol. 38, no. 1, pp. 18–34, 1992.

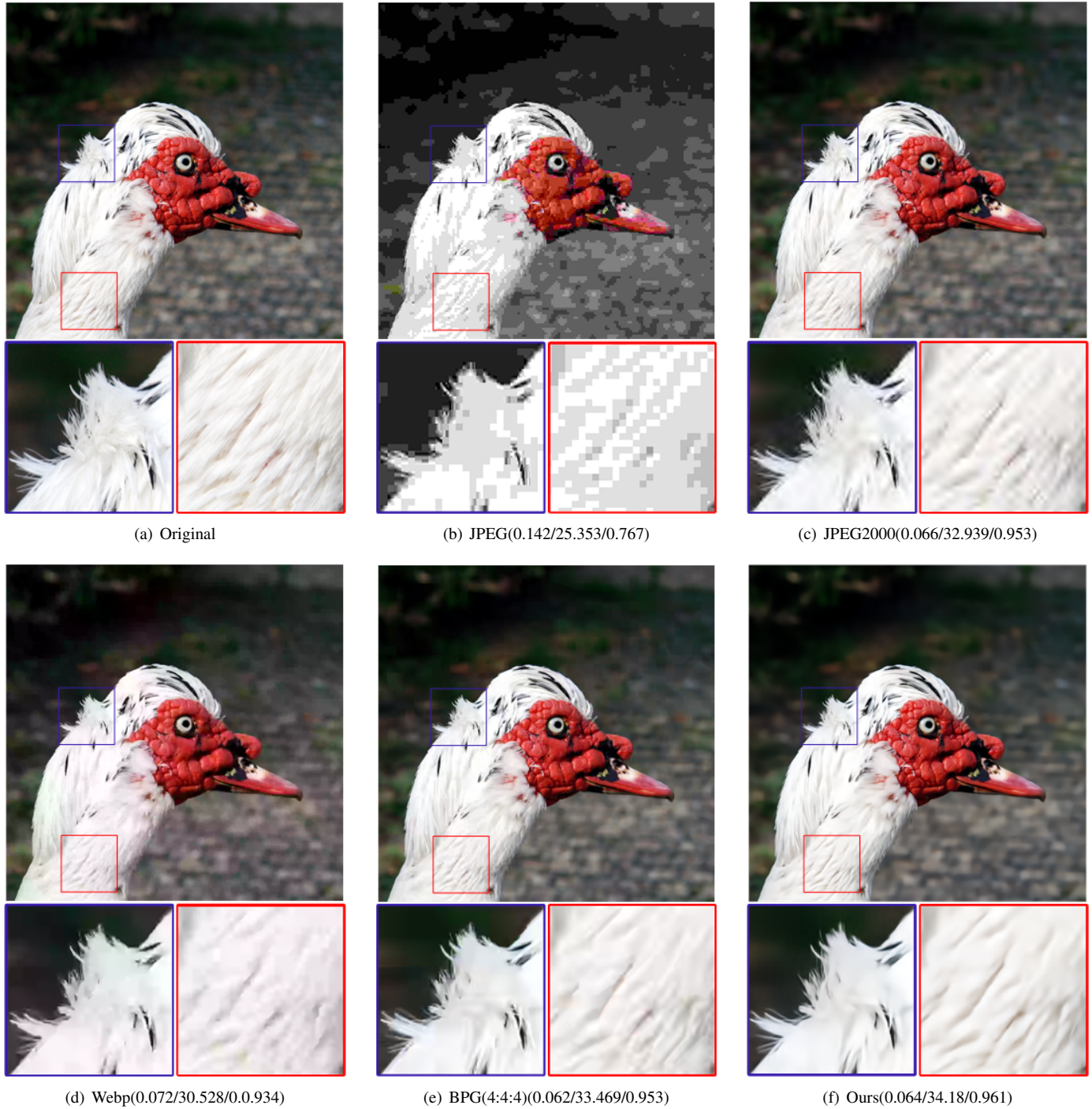


Fig. 9. Example 3 in the Tecnick dataset (bpp, PSNR (dB), MS-SSIM).

TABLE I
PERFORMANCE IMPROVEMENT OF THE TRAINING DATA

Dataset	Name	number filters	λ	objective function	BPP	PSNR	Ms-SSIM
Kodak	Ours	128	0.0032	PSNR	0.1556	29.63 dB	12.59 dB
Kodak	Ours+post-processing	128	0.0032	PSNR	0.1554	29.65 dB	12.59 dB
Kodak	ours	256	0.015	PSNR	0.4408	33.97 dB	16.70 dB
Kodak	Ours+post-processing	256	0.015	PSNR	0.4400	33.98 dB	16.71 dB

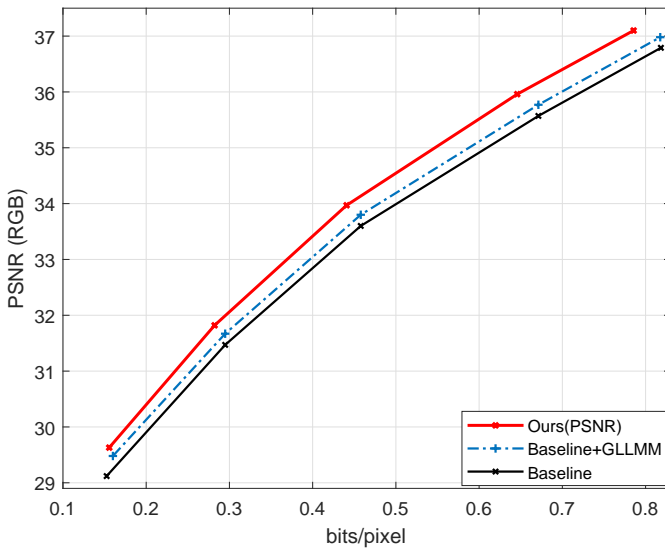


Fig. 10. The R-D curves of several variants of the proposed modules on the Kodak dataset.

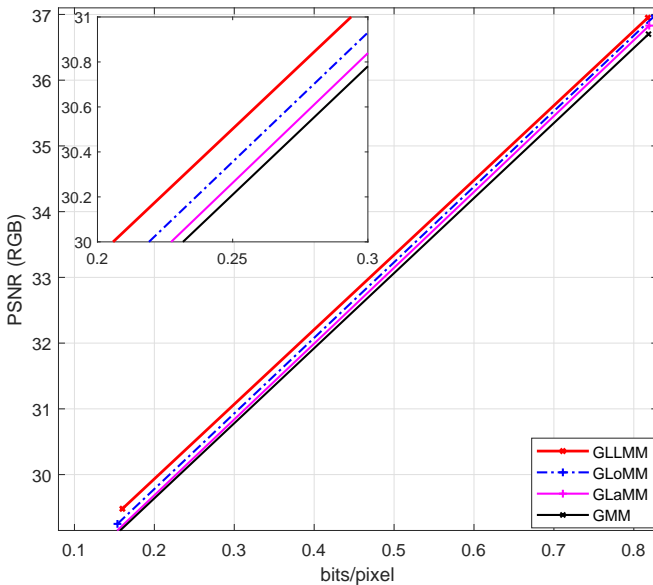


Fig. 11. The R-D curves of several variants of the proposed modules on the Kodak dataset.

- [2] A. Skodras, C. Christopoulos, and T. Ebrahimi, "The jpeg 2000 still image compression standard," *IEEE Signal Processing Magazine*, vol. 18, no. 5, pp. 36–58, 2001.
- [3] G. J. Sullivan, J.-R. Ohm, W.-J. Han, and T. Wiegand, "Overview of the high efficiency video coding (hevc) standard," *IEEE Transactions on Circuits and Systems for Video Technology*, vol. 22, no. 12, pp. 1649–1668, 2012.
- [4] Z. Wang, E. Simoncelli, and A. Bovik, "Multiscale structural similarity for image quality assessment," in *The Thirty-Seventh Asilomar Conference on Signals, Systems Computers, 2003*, vol. 2, 2003, pp. 1398–1402.
- [5] K. He, X. Zhang, S. Ren, and J. Sun, "Deep residual learning for image recognition," in *Proceedings of the IEEE/CVF International Conference on Computer Vision and Pattern Recognition (CVPR)*, June 2016, pp. 770–778.
- [6] G. Toderici, S. M. O'Malley, S. J. Hwang, D. Vincent, D. Minnen, S. Baluja, M. Covell, and R. Sukthankar, "Variable rate image compression with recurrent neural networks," *arXiv:1511.06085*, 2015.
- [7] J. Ballé, V. Laparra, and E. P. Simoncelli, "End-to-end optimization of nonlinear transform codes for perceptual quality," in *2016 Picture Coding Symposium (PCS)*, 2016, pp. 1–5.

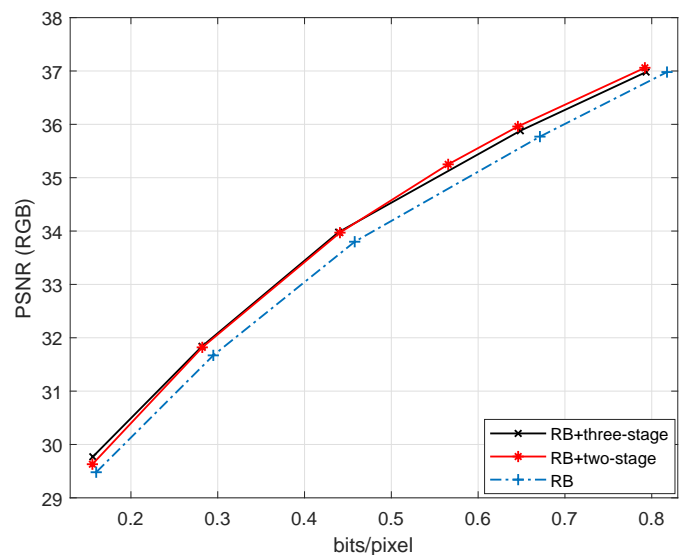


Fig. 12. The R-D curves of several variants of the different concatenated residual modules on the Kodak dataset.

- [8] J. Ballé, V. Laparra, and E. P. Simoncelli, "End-to-end optimized image compression," in *International Conference on Learning Representations*, 2017.
- [9] L. Theis, W. Shi, A. Cunningham, and F. Huszár, "Lossy image compression with compressive autoencoders," in *International Conference on Learning Representations*, 2017.
- [10] M. Akbari, J. Liang, and J. Han, "Dsslic: Deep semantic segmentation-based layered image compression," in *The 2019 IEEE International Conference on Acoustics, Speech and Signal Processing (ICASSP)*, May 2019, pp. 2042–2046.
- [11] S. Santurkar, D. Budden, and N. Shavit, "Generative compression," in *2018 Picture Coding Symposium (PCS)*, June 2018, pp. 258–262.
- [12] O. Rippel and L. Bourdev, "Real-time adaptive image compression," in *Proceedings of the 34th International Conference on Machine Learning*, D. Precup and Y. W. Teh, Eds., vol. 70, 06–11 Aug 2017, pp. 2922–2930.
- [13] J. Lin, M. Akbari, H. Fu, Q. Zhang, S. Wang, J. Liang, D. Liu, F. Liang, G. Zhang, and C. Tu, "Variable-rate multi-frequency image compression using modulated generalized octave convolution," in *2020 IEEE 22nd International Workshop on Multimedia Signal Processing (MMSp)*, 2020, pp. 1–6.
- [14] M. Akbari, J. Liang, J. Han, and C. Tu, "Learned bi-resolution image coding using generalized octave convolutions," in *Proceedings of the AAAI Conference on Artificial Intelligence*, vol. 35, no. 08, Feb 2021, pp. 6592–6599.
- [15] Y. Chen, H. Fan, B. Xu, Z. Yan, Y. Kalantidis, M. Rohrbach, S. Yan, and J. Feng, "Drop an octave: Reducing spatial redundancy in convolutional neural networks with octave convolution," in *Proceedings of the IEEE/CVF International Conference on Computer Vision (ICCV)*, 2019, pp. 3435–3444.
- [16] E. Agustsson, F. Mentzer, M. Tschannen, L. Cavigelli, R. Timofte, L. Benini, and L. V. Gool, "Soft-to-hard vector quantization for end-to-end learning compressible representations," in *Advances in Neural Information Processing Systems*, 2017, pp. 1141–1151.
- [17] O. Rippel and L. Bourdev, "Real-time adaptive image compression," in *International Conference on Machine Learning*, 2017, pp. 2922–2930.
- [18] J. Ballé, D. Minnen, S. Singh, S. J. Hwang, and N. Johnston, "Variational image compression with a scale hyperprior," in *International Conference on Learning Representations*, 2018, pp. 1–23.
- [19] D. Minnen, J. Ballé, and G. D. Toderici, "Joint autoregressive and hierarchical priors for learned image compression," in *Advances in Neural Information Processing Systems*, 2018, pp. 10794–10803.
- [20] D. Minnen and S. Singh, "Channel-wise autoregressive entropy models for learned image compression," in *2020 IEEE International Conference on Image Processing (ICIP)*, 2020, pp. 3339–3343.
- [21] A. van den Oord, N. Kalchbrenner, O. Vinyals, L. Espeholt, A. Graves, and K. Kavukcuoglu, "Conditional image generation with pixelcnn decoders," in *Advances in Neural Information Processing Systems (NIPS)*, 2016, pp. 4797–4805.

- [22] T. Salimans, A. Karpathy, X. Chen, and D. P. Kingma, "Pixelcnn++: Improving the pixelcnn with discretized logistic mixture likelihood and other modifications," in *Intl. Conf. on Learning Representations (ICLR)*, 2017.
- [23] F. Mentzer, E. Agustsson, M. Tschannen, R. Timofte, and L. V. Gool, "Practical full resolution learned lossless image compression," in *Proceedings of the IEEE/CVF Conference on Computer Vision and Pattern Recognition (CVPR)*, 2019, pp. 10629–10638.
- [24] L. Zhou, C. Cai, Y. Gao, S. Su, and J. Wu, "Variational autoencoder for low bit-rate image compression," in *Proceedings of the IEEE Conference on Computer Vision and Pattern Recognition (CVPR) Workshops*, 2018, pp. 2617–2620.
- [25] *The 2019 Workshop and Challenge on Learned Image Compression (CLIC)*, 2018. [Online]. Available: <http://www.compression.cc/>
- [26] J. Lee, S. Cho, and M. Kim, "Joint autoregressive and hierarchical priors for learned image compression," *arXiv:1912.12817*, 2020.
- [27] M. Li, W. Zuo, S. Gu, D. Zhao, and D. Zhang, "Learning convolutional networks for content-weighted image compression," in *Proceedings of the IEEE Conference on Computer Vision and Pattern Recognition (CVPR)*, 2018, pp. 3214–3223.
- [28] H. Liu, T. Chen, P. Guo, Q. Shen, X. Cao, Y. Wang, and Z. Ma, "Non-local Attention Optimized Deep Image Compression," *arXiv e-prints*, p. arXiv:1904.09757, Apr. 2019.
- [29] Z. Cheng, H. Sun, M. Takeuchi, and J. Katto, "Learned image compression with discretized gaussian mixture likelihoods and attention modules," in *Proceedings of the IEEE/CVF Conference on Computer Vision and Pattern Recognition (CVPR)*, 2020, pp. 7939–7948.
- [30] *Kodak PhotoCD dataset*. [Online]. Available: <http://r0k.us/graphics/kodak/>
- [31] *Tecnick dataset*. [Online]. Available: <https://bellard.org/bpg/>
- [32] J. Lee, S. Cho, and S.-K. Beack, "Context-adaptive entropy model for end-to-end optimized image compression," in *International Conference on Learning Representations*, 2019.
- [33] M. Li, W. Zuo, S. Gu, J. You, and D. Zhang, "Learning content-weighted deep image compression," *IEEE Transactions on Pattern Analysis and Machine Intelligence*, pp. 1–1, 2020.
- [34] Z. Cheng, H. Sun, M. Takeuchi, and J. Katto, "Energy compaction-based image compression using convolutional autoencoder," *IEEE Transactions on Multimedia*, vol. 22, no. 4, pp. 860–873, 2020.
- [35] H. Fraunhofer, "Vvc official test model vtm." [Online]. Available: https://vcgit.hhi.fraunhofer.de/jvet/VVCSsoftware_VTM/tree/VTM-5.2
- [36] *Webp*, 2018. [Online]. Available: <https://developers.google.com/speed/webp/>
- [37] *CLIC dataset*. [Online]. Available: <http://www.compression.cc/>
- [38] J. Liu, D. Liu, W. Yang, S. Xia, X. Zhang, and Y. Dai, "A comprehensive benchmark for single image compression artifact reduction," *IEEE Transactions on Image Processing*, vol. 29, pp. 7845–7860, 2020.